493 Prostate Rapid Optical Examination for Cancer STATus (proSTAT): An AI-assisted, 3D Approach to Thoroughly Examine Numerous Levels of Prostate Tissue

Yu-Ching Peng[1], Teh-Ying Chou[2], Yu-Chieh Lin, Yung-An Chen[3], Yen-Yin Lin[4], Yu-Ling Hung, Margaret Chang[5]

[1]Taipei Veterans General Hospital, Taiwan, [2]Taipei Veterans General Hospital, Taipei, Taiwan, [3]JelloX, Taiwan, [4]Taiwan, [5]Hsinchu, Taiwan

Disclosures: Yu-Ching Peng: None; Teh-Ying Chou: None; Yu-Chieh Lin: *Employee*, JelloX Biotech Inc.; Yung-An Chen: None; Yen-Yin Lin: *Employee*, JelloX Biotech Inc.; Yu-Ling Hung: None; Margaret Chang: *Employee*, JelloX Biotech Inc.

Background: Intrinsic opacity and heterogeneity of human tissues have prevented efficient light penetration for signal detection by confocal microscopy. This hurdle has largely been overcome by tissue clearing technology that renders biological tissue transparent. Here we introduce a novel method termed proSTAT, which generates high-resolution 2D and 3D images on thick human prostate tissue without the need of paraffin processing and thin sectioning. Given that proSTAT can generate numerous optical levels by imaging the tissue intact, we further exploit an Artificial Intelligence (AI)-assisted system to localize prostate cancer throughout the z-stacks.

Design: Fifteen tissue cores measuring ~15x2x2 mm per core from five radical prostatectomies were used in this study. The specimens were fixed with 10% formalin, sliced into 100 µm, stained with universal nuclear and cell membrane fluorescence dyes, subjected to tissue clearing solution, and imaged with confocal microscopy. 3D reconstruction and visualization of tumor glands were achieved using the volume rendering function in Avizo software. Three optical slices were manually annotated from the 3D stack images which contained 100 slices. The AI model was trained from these three annotated slices and then inference applied to the rest of slices.

Results: Prostatic adenocarcinoma of various Gleason patterns could be readily identified in tissue cores using proSTAT. Open lumens in Gleason pattern 3 tumors were readily evaluated by tracing a single tumor gland through multiple optical images of the z-stacks (Fig. 1). 3D rendering further provided information on the complexity and heterogeneity of tumor glands. Furthermore, a semi-supervised AI model highlighted tumor areas and enabled calculation of tumor percentage throughout z-stacks (Fig. 2). Totally 79 optical levels were analyzed (3 levels with annotation and 76 with AI inference) and tumor percentage ranged from 14% to 36%, suggesting heterogeneity of tumor distribution along the depth. Calculation of individual cell size revealed significantly larger cells in tumor glands as compared to benign tissue (tumor: 75.8 µm^2 *vs.* benign: 70.0 µm^2).

Figure 1 - 493

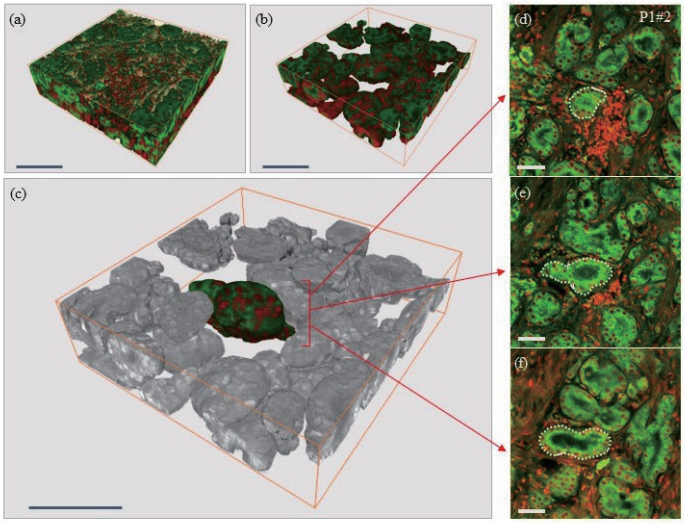

Figure 1 3D reconstructed images of prostate cancer and multiple optical images of the z-stacks.
(a) gross view of tumor region, (b) epithelium segmentation of Fig. 1a, (c) single gland segmentation of Fig. 1b. Bar: 100 µm; Prostate cancer sectioned sample imaging along axial-axis with 15-µm interval in depth of (d) 23-µm, (e) 38-µm, (f) 53-µm. Scale bar: 50 µm, Green: cell membrane. Red: nuclei.

Figure 2 - 493

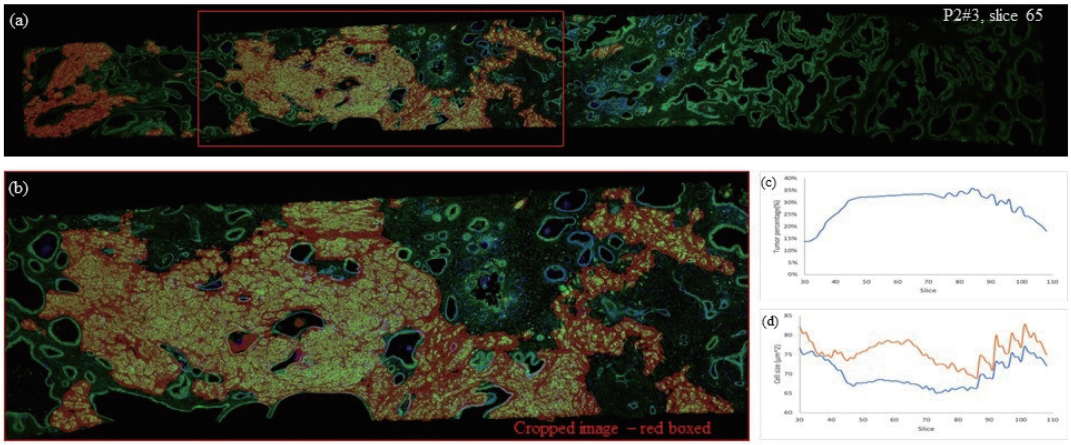

Figure 2 Semi-supervised tumor cell recognition. (a) Whole slide view of the specimen, (b) 2X zooming in (red boxed area in a), (c) pixel-wised tumor percentage with AI model-assisted tumor recognition along the z-stacks, (d) average cell size comparison between tumor/normal cells along the z-stacks. Red: tumor area, Green: cell membrane, Blue: nuclei.

Conclusions: proSTAT presents a rapid, nondestructive method for evaluation of prostate tissue with the advantage of 3D visualization. AI assistance further empowers pathologists to thoroughly examine the entire tissue, providing a potential niche to minimize the risk of missing a small focus of cancer.

494 LZTS2, a Novel and Independent Prognostic Biomarker for Clear Cell Renal Cell Carcinoma: Clinicopathologic Correlation and Immunohistochemical Study

Yue Peng[1], Bradley Stohr[1]
[1]*University of California, San Francisco, San Francisco, CA*

Disclosures: Yue Peng: None; Bradley Stohr: None

Background: Leucine zipper tumor suppressor 2 (*LZTS2*), a putative tumor suppressor gene, has been demonstrated as a negative regulator of microtubule severing during cytokinesis and a negative regulator of the Wnt signaling pathway. In a genetically modified mouse model, deletion of *Lzts2* altered normal ureteric bud branching morphogenesis and caused cystogenesis in mice (Peng, 2011). Cyst-lining cells demonstrated atypical features, closely resembling those observed in mouse models of human clear cell renal cell carcinoma (ccRCC), which were considered as preneoplastic lesions. Notably, high level expression of *LZTS2* is an unfavorable prognostic marker in ccRCC based on RNA sequencing (RNA-seq) data that are available in The Cancer Genome Atlas (TCGA) analyzed by The Human Protein Atlas Project. However, the functions of *LZTS2* in human ccRCC remain largely unknown. Therefore, the aim of this study is to establish an association between *LZTS2* expression and clinicopathologic features of ccRCCs.

Design: Gene expression data by RNA-seq for cohorts of 512 ccRCC cases that have clinical outcome data were extracted from TCGA through cBioPortal. Chi-squared tests, Kaplan-Meier curves and Cox regression models were used to investigate the possible relationship between *LZTS2* mRNA expression levels (z scores) and clinicopathological characteristics as well as patient survival. To examine its cellular localization, we performed LZTS2 antibody staining and scored expression levels (H score) in a pilot study of 35 ccRCCs.

Results: Our analysis of the TCGA data demonstrated that higher LZTS2 expression correlates with worse overall survival and disease specific survival ($p < 0.001$) (Figures 1A and 1B), as well as higher histologic grade ($p = 0.0223$) (Figure 1C). Multivariate Cox regression analysis revealed that high level of LZTS2 is an independent poor prognostic factor for overall survival (HR=5.521 $p = 0.004$) and disease-specific survival (HR=14.881 $p = 0.006$) in ccRCC. By immunohistochemistry, LZTS2 demonstrated predominantly cytoplasmic staining. Four staining patterns were observed as shown in Figure 2. High level cytoplasmic, but not membranous LZTS2 staining correlates with high nuclear grades ($p = 0.041$) in ccRCCs. Thus, LZTS2 IHC staining revealed a range of expression levels and a